J Mater Sci (2009) 44:2566–2572
DOI 10.1007/s10853-009-3335-9

In situ production of Al–TiB_2 nanocomposite by double-step mechanical alloying

Z. Sadeghian · M. H. Enayati · P. Beiss

Received: 2 October 2008 / Accepted: 10 February 2009 / Published online: 9 March 2009

Abstract An in situ Al–TiB_2 nanocomposite was synthesized by mechanical alloying (MA) of pure Ti, B and Al powder mixture in a planetary ball mill. A double-step process was used to prevent the formation of undesirable phases like Al_3Ti intermetallic compound. In the first step, a powder mixture was tailored to obtain nominal Al–90 wt% TiB_2 composition and the second step involved the addition of Al to the mixture in order to achieve Al–20 wt% TiB_2. The structural and thermal characteristics of powder particles were studied by X-ray diffractometry (XRD), scanning electron microscopy (SEM), differential scanning calorimetery (DSC), and transmission electron microscopy (TEM). The results showed that the MA process leads to the in situ formation of nanosized TiB_2 particles in an Al matrix with a uniform distribution. It was also found that the double stage addition of aluminum can prevent the formation of undesirable compounds even after annealing at high temperatures.

Introduction

Aluminum-based metal matrix composites have attracted considerable attention as structural materials in aerospace, automotive, and transportation industries because of their high specific modulus and strength, and superior fatigue and creep resistances [1, 2].

Conventional ceramic materials which are used to reinforce aluminum alloys include carbides, borides, nitrides, and oxides [3]. Among these reinforcing particulates, titanium diboride (TiB_2) has been an attractive candidate since it exhibits high melting point (2900 °C), high modulus (565 GPa), high hardness (2500 HV), and good thermal stability [4]. TiB_2 particles are commonly incorporated into the aluminum matrix via casting and powder metallurgy processes. The main problems of these methods are agglomeration and inhomogeneous distribution of TiB_2 particles in the matrix [5–7].

In order to overcome these limitations in situ processes have recently received much attention because of their interesting characteristics. By the in situ formation of metal matrix composites (MMCs), a more homogenous microstructure can be achieved. Moreover, the reinforcements made by in situ reactions show a clean interface of reinforcement matrix and small size of particles resulting in better mechanical properties [8–11]. For an in situ process to take place, an exothermic reaction is needed to form the reinforcement. It is also essential for the reinforcement to be thermodynamically stable in the matrix. Among all the in situ reinforcements for aluminum, Al_2O_3, TiC, and TiB_2 have been most widely used [12]. TiB_2 is of particular interest because it is compatible with the aluminum matrix and does not react with the aluminum after formation. A variety of processing techniques have been developed for in situ production of MMCs during the past decade. Traditionally, in situ MMCs such as Al–TiB_2 composites have been produced by several processing routes such as exothermic dispersion (XD), reactive hot pressing (RHP), self propagating high temperature synthesis (SHS), various

Z. Sadeghian (✉) · P. Beiss
Institute for Materials Applications in Mechanical Engineering, RWTH Aachen University, 52062 Aachen, Germany
e-mail: Z.Sadeghian@iwm.rwth-aachen.de

Z. Sadeghian · M. H. Enayati
Department of Materials Engineering, Isfahan University of Technology, Isfahan 84156-83111, Iran

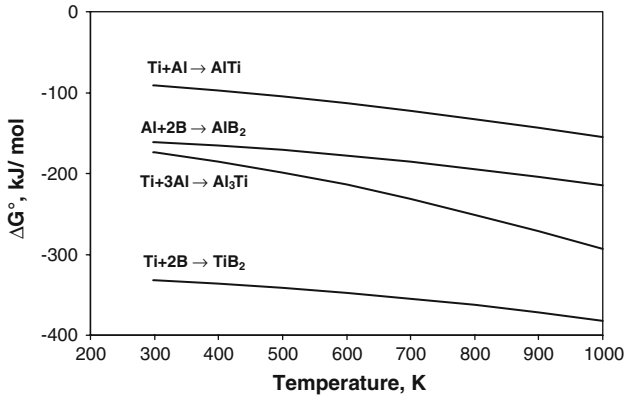

Fig. 1 Variation of Gibb's free energy of TiB_2, AlTi, and Al_3Ti compounds with temperature

casting techniques, i.e., reactive squeeze casting, rapid solidification processing (RSP), and mechanical alloying (MA) [13–18].

MA technique has been extensively used to fabricate in situ ceramic particle reinforced MMCs. It is shown that by this process some reactions, which are difficult to occur under conventional conditions, can be induced [18, 19]. In situ TiB_2 particle-reinforced copper composites have been fabricated by means of the MA process, followed by a suitable heat treatment [20]. During the in situ synthesis of Al–TiB_2 composites in Al–Ti–B, Al–TiO_2–B, and Al–TiO_2–B_2O_3 systems formation of Al_3Ti intermetallic compound is reported by some investigators [21–23]. Al_3Ti is a brittle compound due to its tetragonal structure and platelet morphology [24, 25]. This intermetallic compound has been reported to considerably reduce the fatigue life of composites owing to the promotion of microscopic cracking during cyclic deformation [26]. Therefore, it is of interest to eliminate the formation of Al_3Ti intermetallic compound.

According to the thermodynamic data, TiB_2 is the most stable phase in comparison to TiAl and Al_3Ti intermetallic compounds (Fig. 1) [27]. In our previous article, it was shown that a high Al content in the initial mixture reduced the direct contact and as a result the reaction between Ti and B in the mixture [28]. In order to overcome this problem in this study, a route is proposed for producing TiB2 aluminum matrix nanocomposite via MA technique, which additionally prevents the formation of undesirable Al3Ti intermetallic compound.

Experimental procedures

Commercially available Al (99.8%), Ti (99.9%), and B ($\geq$ 99%) powders were used as starting materials. The aluminum powder with an average particle size of 63 μm was supplied from ECKA Granulate (Velden, Germany). The titanium powder with a particle size of 40–60 μm was obtained from GKN Sinter Metal Filters (Radevormwald, Germany), and the Merck boron powder (Darmstadt, Germany), had a particle size of about 2 μm.

Powder mixtures were milled by a Fritsch planetary ball mill with a rotating speed of 360 rpm. The ball to powder weight ratio was chosen to be 10:1 and the diameter of the chromium steel balls was 15 mm. The hardened chromium steel vial was evacuated and filled with pure argon gas to prevent oxidation during the MA process. In order to avoid severe adhesion of aluminum powder to the balls and the vial surfaces, 1 wt% zinc stearate was added to the mixture as a process control agent.

A double-step process was used to obtain Al–TiB_2 MMC. In the first step, a mixture of 62 wt% Ti–28 wt% B was milled with a small amount of Al (10 wt%) up to 20 h to prevent the formation of unwanted phases such as Al_3Ti and AlTi. This powder was further milled for 20 h (total milling time of 40 h) with additional aluminum powder to achieve the Al–20 wt% TiB_2. At selected times, the milling was interrupted and the vial was cooled to room temperature for sampling.

A SEIFERT 30033 PTS diffractometer (40 kV and 40 mA) employing monochromatic Cu Kα1 radiation (λ = 0.15406 nm) was used to investigate the structural changes during MA and heat treatment of the powder. XRD scans were performed with a step size of 0.05° and a dwell time per step of 20 s. The cross-sectional microstructures of the powder particles together with spot analysis were studied with the aid of a LEO 1450 VP scanning electron microscope (SEM) at an accelerating voltage of 15 kV with an energy dispersive X-ray spectrometer (EDX). In order to evaluate the thermal behavior and stability of the powder during subsequent fabrication processes, e.g., sintering, differential scanning calorimetery (DSC) experiment was conducted using a Netzsch 402 tgermal analyzer. The sample was placed in a platinum crucible and heated under argon flow with a heating rate of 15 °C min^{-1} over the 25–550 °C temperature range.

Transmission electron microscopy experiments were conducted using a FEI Tecnai G2 TEM instrument working at 200 kV. The TEM sample was prepared by embedding the powder particles in a specialized copper epoxy matrix. A thin film with 100-nm thickness was then cut from the mounted powder using Focused ion beam (FIB) technique. For the TEM analysis, high-resolution transmission electron microscopy (HRTEM) and scanning transmission electron microcopy (STEM) techniques were used.

Results and discussions

Figure 2 shows the X-ray diffraction patterns of the Al–62 wt% Ti–28 wt% B, and Al–20 wt% TiB_2 powders after

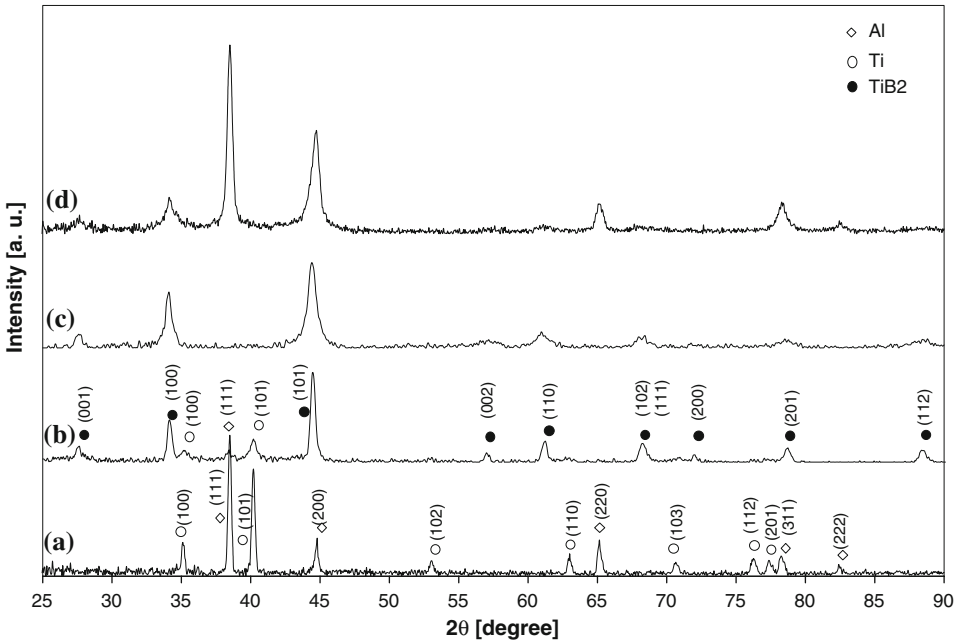

Fig. 2 XRD patterns of Al–62 wt% Ti–28 wt% B powder mixture: (a) as-received, (b) as-milled for 10 h, (c) as-milled for 20 h and (d) final powder obtained from the first step + 20 h ball milling with addition of elemental Al powder

different milling times. After 10 h, the peaks related to TiB_2 can be observed on the X-ray pattern (Fig. 2b). No peak shift was observed for titanium and aluminum indicating that no solid solution was formed during MA process. It is worth mentioning that in some experiments, a self propagating reaction occurred in the 10-h milled powder as soon as the vial was opened in air. This may arise from the exothermic oxidation reaction of the clean and active surfaces of the Al powder particles leading to the initiation of a self sustaining reaction between Ti and B. This observation can support the idea that the local temperature raise during MA of the Al–Ti-B powder mixture tends to a SHS process. In contrast, Tang et al. reported a diffusional mechanism for the formation of TiB_2 during MA of elemental Ti and B powders [29].

As shown in Fig. 2c after 20 h of milling time, no traces of Ti peaks were observed on XRD patterns suggesting that Ti–B solid state reaction is completed at this stage. The lack of Al peaks on XRD pattern can be due to the several effects including high strain level induced in the Al lattice, nanosized Al grains and lower X-ray scattering intensity of Al compared to the other constituents. All these effects reduced the XRD intensity of Al peaks.

Lu et al. did not obtain TiB_2 directly during the MA of Al–Ti-B powder mixture. They reported that TiB_2 can be achieved only after annealing of mechanically alloyed powder [22, 30].

After milling for 20 h, elemental aluminum powder was added and MA continued up to 20 h in order to achieve a nominal composition of Al–20 wt% TiB_2. As can be seen in Fig. 2d, no structural change occurred in the powder. Both Al and TiB_2 peaks became broader due to the refinement of grain size and enhancement of lattice strain. The grain size of the aluminum matrix and TiB_2 was obtained from XRD analysis using Williamson–Hall (WH) equation [31]:

$$\Delta(2\theta)\cos\,\theta = \frac{0.9\lambda}{D} + 4\varepsilon\,\sin\,\theta \qquad (1)$$

where $\Delta(2\theta)$ is the full width at half maximum (FWHM) of the Bragg peaks (in radians), θ is the Bragg angle of the analyzed peak, λ is the wavelength of the X-rays used in nanometers (0.154056 nm for Cu Kα1), D is the average crystallite size, and ε is the average strain. For each of the phases, three reflections within a 2θ range of 20° to 90° were used to construct a linear plot of $\Delta(2\theta)\cos\,\theta$ versus $\sin\,\theta$, from which the average grain size and internal strain were obtained using Eq. 1. The average grain size and internal lattice strain of aluminum matrix and TiB_2 particles are listed in Table 1. After 40 h of MA, the TiB_2

Table 1 Average grain size and lattice strain values of Al and TiB_2 calculated by the WH equation

Sample	Crystalline size (nm)		Lattice strain (%)	
	Al	TiB_2	Al	TiB_2
Al–90 wt% TiB_2 (first step, 20 h milling)	–	19	–	0.02
Al–20 wt% TiB_2 (second step, a total milling time of 40 h)	16	14	0.215	0.115
Al–20 wt% TiB_2 from the second step (after annealing in DSC)	30	16	0.165	0.062

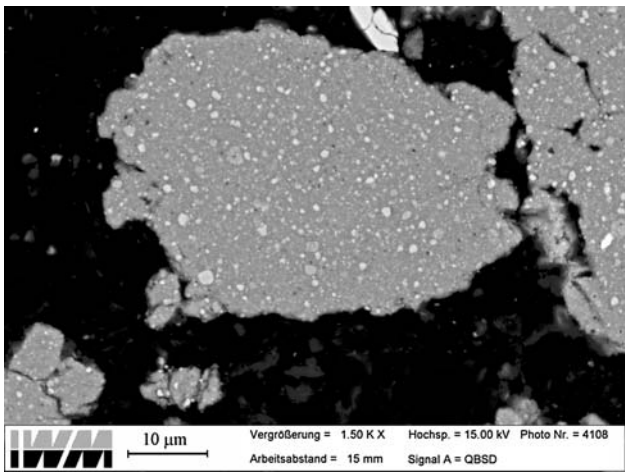

Fig. 3 A typical cross-sectional SEM micrograph of Al–20 wt% TiB_2 powder particle obtained from the second step after a total milling time of 40 h

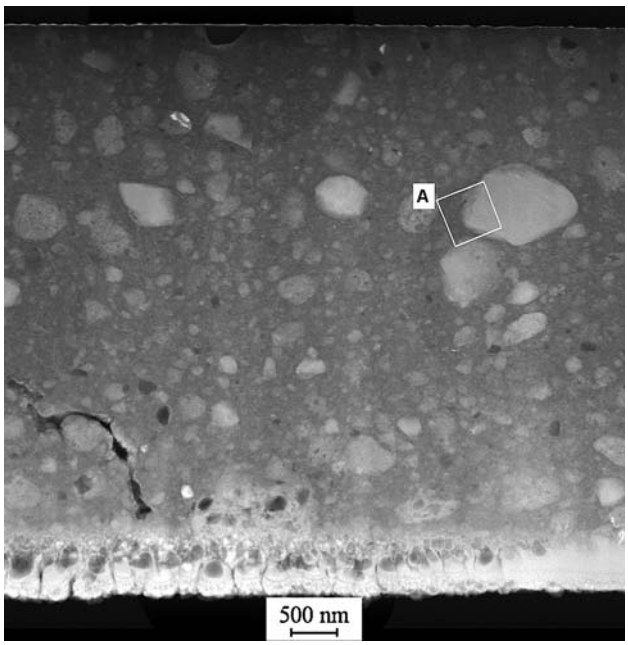

Fig. 5 STEM image of an Al–20 wt% TiB_2 powder particle obtained from the second step after a total milling time of 40 h

particles and aluminum matrix achieved a grain size of 14 and 16 nm, respectively.

Figure 3 shows a typical cross sectional SEM micrograph of the final Al–20 wt% TiB_2 powder particles after a total milling time of 40 h. EDS analysis indicated that the bright particles are TiB_2 phase (Fig. 4). As can be seen, a fine and uniform distribution of TiB_2 particles within the aluminum matrix is obtained although most of the TiB_2 particles appeared to be too small to be observed on SEM.

A higher magnification of the final Al–20 wt% TiB_2 composite powder obtained by STEM is presented in Fig. 5. Most of the TiB_2 particles have a size range of several nanometers up to 100 nm and only a few of particles are about 500 nm to 1 µm. The approximate average TiB_2 particle size measured using image analysis software was about 90 nm.

The TEM images of the powder after the second step are presented in Fig. 6. The continuous ring for selected area diffraction pattern (SADP), along with the dark field image reveal the nanocrystalline characteristics of the microstructure. According to the dark-field image (Fig. 6b), the size of the grains was measured to be in the range of

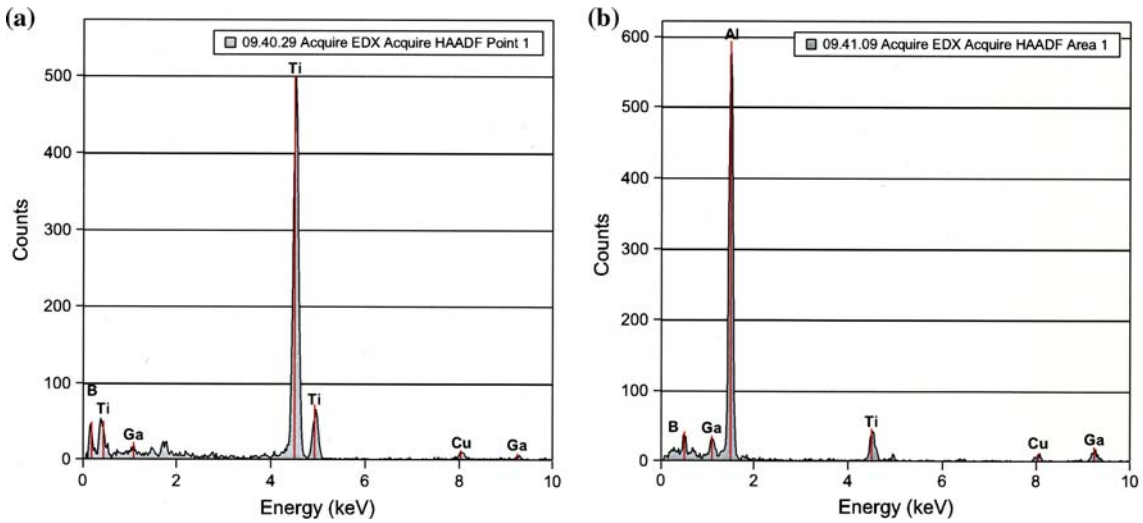

Fig. 4 EDS analysis from: **a** bright area and **b** the matrix in Fig. 3

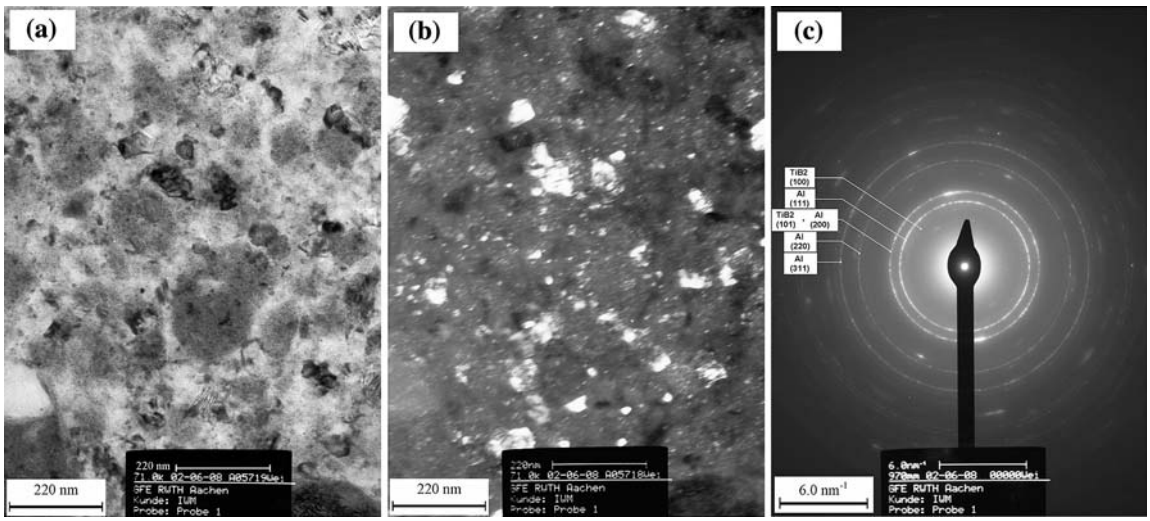

Fig. 6 TEM images of Al–20 wt% TiB_2 powder particles obtained from the second step after a total milling time of 40 h: **a** bright field image, **b** dark field image, and **c** SADP pattern

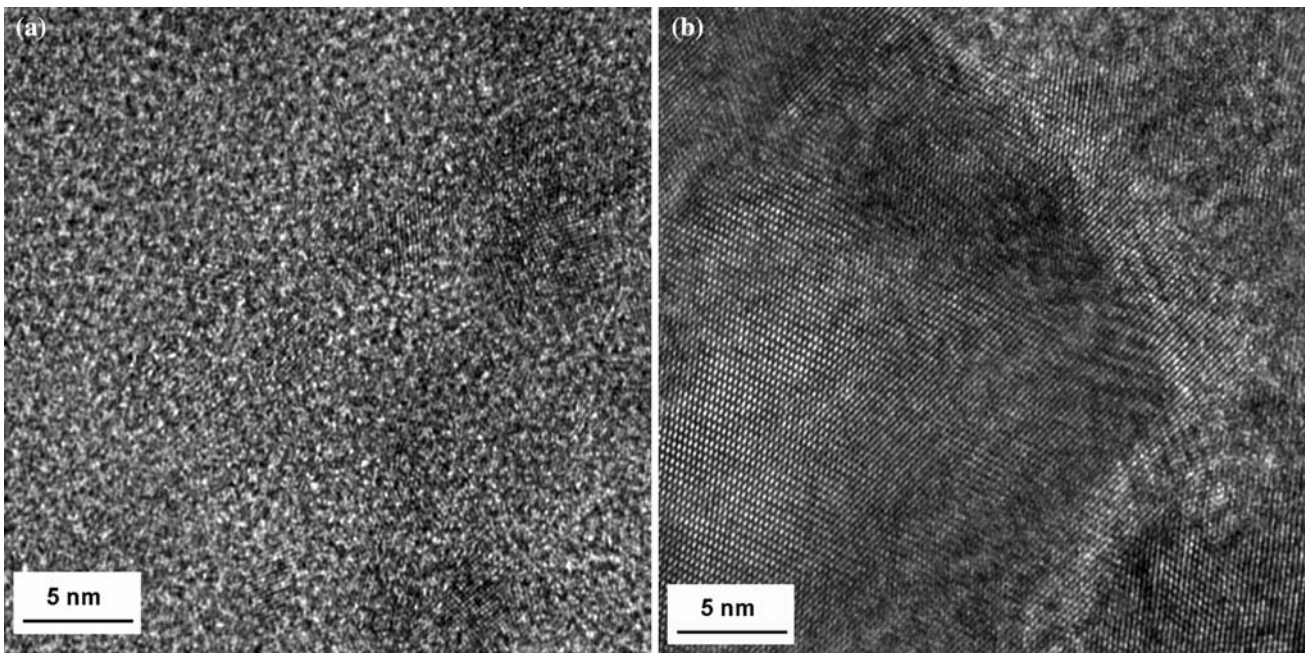

Fig. 7 HRTEM images of Al–20 wt% TiB_2 powder obtained from the second step after a total milling time of 40 h showing: **a** individual mono crystal TiB_2 particles and **b** a large TiB_2 particle consisting of nano scale grains (region A in Fig. 5)

2–110 nm with an average of 20 nm which is in good agreement with the values obtained from the WH equation. Since both Al and TiB_2 diffraction lines exist in the SADP it is difficult to separate the dark-field image for TiB_2 and Al.

The nano scale size of TiB_2 was further confirmed by HRTEM observations. Figure 7 shows the HRTEM image of TiB_2 particles after the second step. The size of TiB_2 particles in some regions was as small as 5 nm. The HRTEM investigation also showed that even the large particles, particle (A) in Fig. 5, are an agglomeration of several nanosized TiB_2 particles (Fig. 7b).

The DSC trace of powder particles taken after the second step (Fig. 8) represents no exothermic peak up to

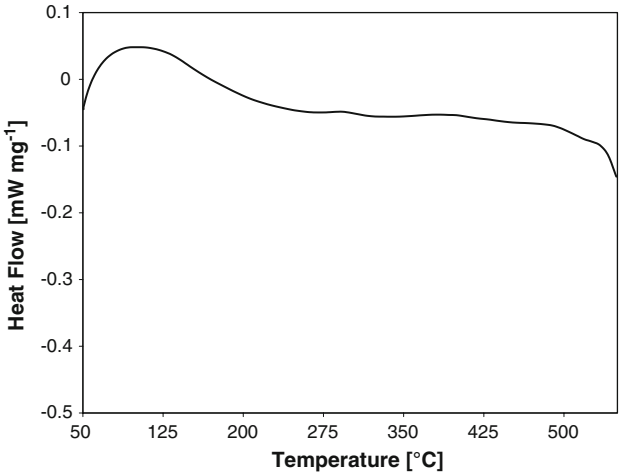

Fig. 8 DSC trace up to 550 °C of the Al–20 wt% TiB_2 powder obtained from the second step after a total milling time of 40 h

550 °C. Furthermore, the XRD patterns taken after the DSC run remained unchanged compared to that for the as-milled powder (Fig. 9). No traces of undesirable phases such as Al_3Ti, were observed on XRD patterns after annealing in DSC. Lu et al. reported that during the heat treatment of as milled Al–Ti–B powder mixture, Al_3Ti phase is formed in the aluminum matrix along with TiB_2 [30]. The results obtained here showed that by double stage addition of aluminum one, can prevent the formation of undesirable compounds even after annealing at high temperatures. The average grain size of TiB_2 did not increase during annealing in DSC; in contrast, the grain size of the aluminum matrix grew from 16 to 30 nm (Table 1). As a result, the Al–TiB_2 nanocomposite powder is expected to have good thermal stability during subsequent consolidation process. The slight increase in the grain size of aluminum matrix indicates that TiB_2 nanoparticles distributed in an aluminum matrix can effectively prevent the grain growth.

Conclusions

Al–TiB_2 nanocomposite powder was synthesized by a double-step MA process of elemental powders. TEM and HRTEM observations showed that TiB_2 particles with a size of 5 to 100 nm and uniform distribution were formed in the Al matrix after a total milling time of 40 h. No traces of undesirable phases such as titanium aluminides were observed even after annealing of the powder. The resulting Al–TiB_2 nanocomposite had good thermal stability upon heating.

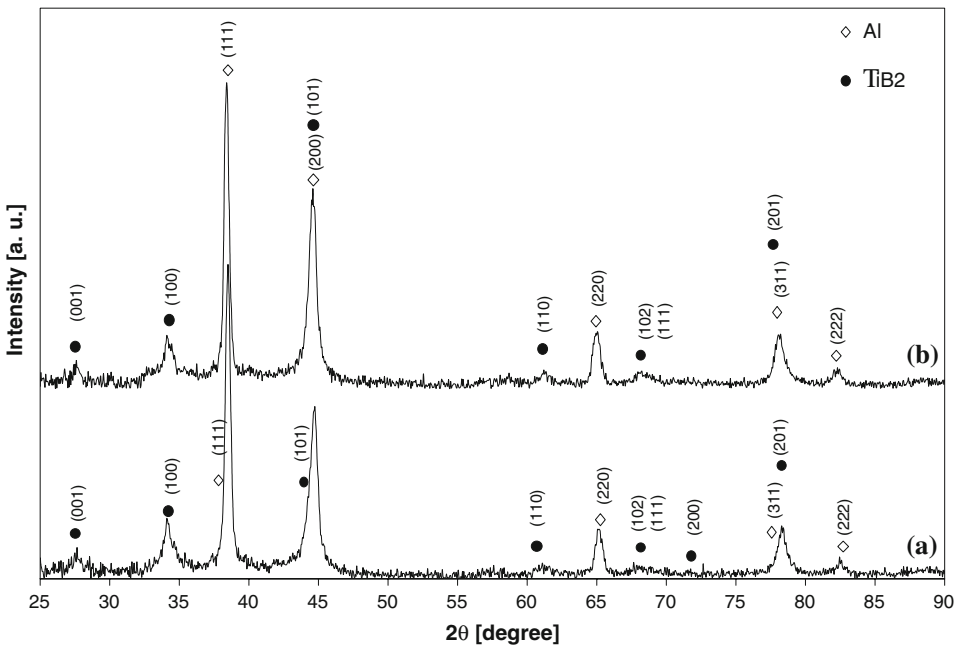

Fig. 9 XRD patterns of Al–20 wt% TiB_2 powder obtained from the second step after a total milling time of 40 h: (a) as milled and (b) after subsequent annealing in DSC up to 550 °C

Acknowledgement Z. Sadeghian's sincere thanks go to the Deutscher Akademischer Austauschdienst (DAAD) for supporting the stay in Germany.

References

1. Miracle DB, Donaldson SL (2001) ASM handbook, vol 21. ASM International, Materials Park, Ohio, p 1020
2. Srivatsan TS, Lewandowski J (2007) In: Winston S et al (eds) Advanced structural materials: properties, design optimization, and applications. CRC Press, New York
3. Davis JR (1993) Aluminum and aluminum alloys, ASM specialty handbook. ASM International, Materials Park, Ohio
4. Munro RG (2000) J Res Natl Inst Stand Technol 105:709
5. Tjong SC, Lau KC (1999) Compos Sci Technol 59:2005
6. Watson IG, Forster MF, Lee PD et al (2005) Composites A 36:1177
7. Zhu D, Wu G, Chen G et al (2008) Mater Sci Eng A 487:536
8. Lakshmi S, Lu L, Gupta M (1998) J Mater Process Technol 73:160
9. Kumar S, Sarma VS, Murty BS (2008) Mater Sci Eng A 476:333
10. Feng CF, Froyen L (2000) J Mater Sci 35:837. doi:10.1023/A:1004729920354
11. Brinkman HJ, Duszczyk J, Katgerman L (1997) Scripta Mater 37:293
12. Ralph B, Yuen HC, Lee WB (1997) J Mater Process Tech 63:339
13. Mitra R, Chiou WA, Fine MA et al (1993) J Mater Res 8:2380
14. Gotman I, Koczak MJ, Shtessel E (1994) Mater Sci Eng A 187:189
15. Taheri-Nassaj E, Kobashi M, Choh T (1996) Scripta Mater 34:1257
16. Tee KL, Lu L, Lai MO (2001) Mater Sci Technol 17:201
17. Ma ZY, Tjong SC (1997) Metall Mater Trans A 28:1931
18. Tjong SC, Ma ZY (2000) Mater Sci Eng A 29:49
19. Suryanarayana C (2001) Prog Mater Sci 46:1
20. Biselli C, Morris DG, Randall N (1994) Scripta Metall Mater 30:1327
21. Lu L, Lai MO, Su Y et al (2001) Scripta Mater 45:1017
22. Lu L, Lai MO, Wang HY (2000) J Mater Sci 35:241. doi:10.1023/A:1004789910279
23. Zhu H, Wang H, Ge L (2008) Wear 264:967
24. Watanabe Y, Eryu H, Matsuura K (2001) Acta Mater 49:775
25. Nakamura M, Kimura K (1991) J Mater Sci 26:2208. doi:10.1007/BF00549190
26. Tjong SC, Wang GS, Mai YW (2005) Compos Sci Technol 65:1537
27. Barin I (1989) Themodynamical data of pure substances. Wiley-VCH, Weinheim
28. Sadeghian Z, Enayati MH, Beiss P (2008) In: Krueger G (ed) Proceeding of Euro PM2008, Mannheim, p 3, 29 September–1 October 2008
29. Tang W, Zheng Z, Wu Y et al (2006) Trans Nonferr Metal Soc 16:613
30. Lu L, Lai MO, Xiao Ping N et al (1998) Z Metallkd 89:567
31. Suryanarayana C, Norton MG (1998) X-ray diffraction: a practical approach. Plenum Press, New York